JCEC
THE JOURNAL OF ENGINEERING AND EXACT SCIENCES

OPEN ACCESS

The Journal of Engineering and Exact Sciences – jCEC, Vol. 09 N. 09 (2023)
journal homepage: https://periodicos.ufv.br/jcec
eISSN: 2527-1075
ISSN: 2446-9416

CT and MRI image fusion based on variance and pixel significance

Article Info:
Article history: Received 2023-08-02 / Accepted 2023-10-01 / Available online 2023-10-05
doi: 10.18540/jcecvl9iss9pp16619-01e

Boubakeur Latreche
ORCID: https://orcid.org/0009-0007-9367-3368
Telecommunications and smart systems Laboratory, Faculty of Science and Technology, University of Djelfa, Djelfa 17000, Algeria
E-mail: b.latreche@univ-djelfa.dz

Abstract

In the medical imaging field, images are obtained using various modalities, including the computed tomography procedure and the magnetic resonance imaging procedure. In which every image contains different information from the other image. For better treatment and diagnosis of a patient, a single composite image must be created by fusing all the pertinent data. This process is known as image fusion. We present an innovative and effective image fusion technique utilizing ILWT and DCT for combining brain-related medical images acquired through there are two steps to this strategy. First, the variance is employed as a contrast evaluation in the DCT domain to combine the approximation coefficients generated by the ILWT decomposition. Second, the coefficients representing the fine details are combined by finding the ideal weighted average based on the importance of the pixels in the ILWT domain. Our method is straightforward, making it simple and suitable for deployment in real-time applications. The experimental results demonstrate our method's outstanding performance with regard to both result quality and in contrast to a number of picture fusion techniques.
Keywords: Image fusion. medical imaging. ILWT. DCT.

Nomenclature

CT: Computed Tomography
MRI: Magnetic Resonance Imaging
ILWT: Integer Lifting Wavelet transform
DCT: Discrete Cosine Transform
HIS: Intensity Hue Saturation
PCA: Principal Component Analysis
BT: Brovey Transform
DWT: Discrete Wavelet Transform
LAP: Laplacian Pyramid
2-D: Two Dimensional
AC: Alternating Current
DC: Direct Current
LL: Low-Low
LH: Low-Hight
HL: Hight-Low
HH: Hight-Hight
CV: Consistency Verification
SB: Sub Band
WT: Weight factor

SIDWT: Shift Invariant Discrete Wavelet Transform
Max: Maximum
AV: Average
STD: Standard deviation
He: Entropy
AG: Average Gradient
SF: Spectral Frequency
$Q^{\frac{AB}{F}}$: Edge-based similarity metric
$L^{\frac{AB}{F}}$: Total loss of information

1. Introduction

Images in the field of medical imaging contain a wealth of unique information on human tissues and organs. They also contain visual data regarding structural images, such as those produced by MRI and CT scans (Azam *et al*., 2022). In general, the CT picture can clearly communicate information about human bones but is unable to discern the intricacies of soft tissue (Starmans *et al*., 2022). In contrast, the MRI can express soft tissue information clearly but cannot be sensitive to human bones (Singh *et al*., 2018). To get a more accurate diagnosis, doctors can merge the MRI and CT scans of the same patient who has a tumor (Ursuleanu *et al*., 2021), but stopping this process would be improper and tedious. Most importantly, people with various levels of knowledge reach disparate conclusions when faced with similar images. Consequently, the development of an image fusion system is imperative to ameliorate diagnostic consistency and mitigate the physician's workload burden. (Wan *et al*., 2021).

The operation of integrating many images into a smaller set is known as image fusion (Bhalla *et al*., 2022). A single merged image is typical. Compared to each of the initial source images, the composite image offers a more precise representation of the scene (Latreche *et al*., 2018). From the 1970s of the 20th century to today, various medical imaging fusion techniques have been developed (Alseelawi *et al*., 2022; Ganasala *et al*., 2020; Hou *et al*., 2019; Li *et al*., 2021; Na *et al*., 2018). The easier technique of image fusion is done in the spatial domain by taking the maximum, minimum or averaging of each comparable pixel of the input images (Liu *et al*., 2020). However, this technique frequently results in unwanted outcomes, such as diminished contrast.

Other spatial domain techniques in accordance with the intensity hue saturation (IHS) model (Choi, 2006), principal component analysis (PCA) (Metwalli *et al*., 2009) and Brovey transform (BT) (Gharbia *et al*., 2014) are quick, straightforward, and simple to use. They do, however, result in spectral deterioration and blurring, which lower the contrast of the final image.

So far, in the fusion of medical images, several methods in the transform domain have been used, like pyramids (Sahu *et al*., 2014), discrete cosine transform (DCT) (Phamila *et al*., 2014), and discrete wavelet transform (DWT) (Singh *et al*., 2014; Vijayarajan *et al*., 2015). In the transform domain, source images undergo conversion into various domains (from spatial to frequential), where the fused coefficients are received by combining the representations of source images employing a particular fusion criterion (Diwakar *et al*., 2021). Ultimately, the resulting fused image is generated by applying the drawback transform to the combined coefficients.

A well-known multi-resolution tool, the Laplacian pyramid (LAP) method, is commonly employed in the domain of medical image fusion, but this approach lacks information direction. The DCT image fusion methods suffer from blurring and blocking artifacts in the fused images because each start image is partitioned into non-overlapping 8×8 blocks. Unfortunately, the DWT is not shift-invariant because of the reduction of sampling used in its computation. Also, there is a shortage

of information direction. This results in moving artifacts in interframe, ringing artifacts in intraframe and pseudo-Gibbs phenomena (Li *et al*., 2017).

In this research, we suggest an effective image fusion approach for the CT and the MRI medical images to generate a complete image that includes both clear soft tissue and bone tissue information in order to help the doctors in the careful diagnosis of the illness and to decide the needed therapy in harmony with the patient's state. This method involves two fusion steps. The first fusion step is performed in the DCT domain, and the second step is performed in the integer to integer lifting scheme of the wavelet domain. The suggested technique has been examined on MRI and CT medical image modalities and further compared with some other approaches in both quantitative and qualitative terms. The outcomes and comparative analyses unequivocally demonstrate the superior efficacy of our innovative introduced algorithm relative to the comparative algorithms.

The subsequent sections of this manuscript are structured as follows: Section 2 presents methods used in this paper, such as DCT and ILWT. Section 3 explains the suggested fusion scheme, this approach is grounded on both ILWT and DCT. Section 4 details the experiments results. Section 5 will finally wrap up this paper.

2. Methods

2.1 Discrete Cosine Transform

A mathematical transformation known as the 2D-DCT converts a two-dimensional array of data into a collection of coefficients that represent the frequency components of the data. The 2D-DCT is often used in the JPEG image compression, it can be used for various image processing purposes and multimedia applications, including image fusion. DCT comes in essentially two varieties. The 2-D DCT is used because an image is thought of as a 2-D matrix.

The 2-D DCT of an $N \times N$ image block $b(i,j)$ is denoted by Equation 1:

$$F(k,l) = \frac{2c(k)c(l)}{N} \sum_{i=0}^{N-1} \sum_{j=0}^{N-1} b(i,j) \times \cos\left[\frac{(2i+1)k\pi}{2N}\right] \times \cos\left[\frac{(2j+1)l\pi}{2N}\right] \quad (1)$$

With $k, l = 0,1, \dots, N-1$ and

$$c(k) = \begin{cases} \frac{1}{\sqrt{2}}, & k = 0, \\ 1, & k \neq 0. \end{cases} \quad (2)$$

The drawback 2-D DCT transformer can be used to recreate the original image from its DCT coefficients as follows in Equation 3:

$$b(i,j) = \sum_{k=0}^{N-1} \sum_{l=0}^{N-1} \frac{2c(k)c(l)}{N} \times F(k,l) \times \cos\left[\frac{(2k+1)i\pi}{2N}\right] \times \cos\left[\frac{(2l+1)j\pi}{2N}\right] \quad (3)$$

With $i, j = 0,1, \dots, N-1$. In (1), all coefficients $F(k,l)$ represent the alternating current components (AC), whereas the $F(0,0)$ value corresponds to the direct current component (DC).

2.2 Integer Lifting scheme of Wavelet Transform

As is common knowledge, the Fourier transform underlies the classical wavelet transform, which filters the original signal using high-pass and low-pass filters. The result is then sub-sampled to provide sub-bands for detail and approximation, respectively. This operation requires more time for processing and large amounts of memory due to its computational complexity. To overcome these problems, the lifting scheme of the wavelet transform is recommended in (Sweldens *et al*., 1998).

LWT is referred to as the next stage in the evolution of wavelet transforms. It can directly compute the wavelet transform without relying on the Fourier transform. Unfortunately, the resulting signal of the lifting scheme is coded in floating-point numbers format, which usually obstructs strictly reconstructing the original signal. The authors in (Calderbank *et al*., 1998) resolve this problem by proposing an integer-to-integer implementation of the wavelet transform lifting scheme. The implementation of the lifting wavelet involves three stages, as demonstrated below (Latreche *et al*., 2018):

Split: This process creates a basic wavelet known as "the lazy wavelet", which splits the initial signal into odd and even patterns.

$$split(x_i) = (s_i^0, d_i^0) \tag{4}$$

Predict: here, using the correlation in the original signal, the even sequence is utilized to forecast the odd sequence. This process yields a result resembling the convolution wavelet output high-pass filter.

$$d_i^n = d_i^{n-1} - P(s_i^{n-1}) \tag{5}$$

Update: In this step, the updated event sequence can be computed by adding the even sequence and the modified odd sequence. This step produces a result that is similar to the low-pass filter output of coevolution wavelets.

$$s_i^n = s_i^{n-1} - U(d_i^n) \tag{6}$$

The lifting scheme's ability to quickly perform the inverse (drawback) transform and to give the right context for developing the integer-to-integer implementation are both significant benefits. Quantizers are positioned for this immediately following the updating and prediction processes, as well as before the modification of the odd and even sequence values. These processes are broken down for easier comprehension in Figure 1.

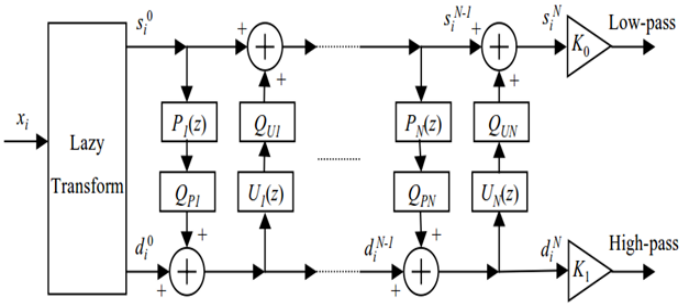

Figure 1 - The general flowchart of a forward ILWT.

3. The suggested Image fusion scheme

In this part, we suggest an innovative image fusion technique based on the ILWT and the DCT for CT and MRI medical imaging. There are two stages to the fusion process. Using the two-dimensional ILWT, the input images decompose into sub-bands for both detail and approximation. First, by selecting variance as an appropriate contrast measure, the approximation sub-bands from each source image are merged within the domain of the discrete cosine transform. Then, their fusion replaces these approximation sub-bands. Second, for the purpose of combining the detail sub-bands, the best weights are determined adaptively by determining the importance of each pixel based on the correlation between the overall coefficient levels.

Here, consider that we have two source images: CT and MRI. With the objective of generating the output fused image, denoted as F, we initiate the process by subjecting the source images (CT or MRI) to ILWT. As a result, we have, for each source image, four bands (LL_1, HL_1, LH_1, HH_1) during the initial-level decomposition. Which the LH_1, HL_1 and HH_1 sub-bands refer to the detail information (high frequencies) in the vertical, horizontal, and diagonal orientations. while LL_1 represents a reduced-size rendition of the original input image (low frequencies) itself.

Constantly, the *LL* approximation sub-band is employed in the decomposition process. In the 3rd level, for any source image, we obtain ten sub-bands. Where (LH_1, LH_2, LH_3), (HL_1, HL_2, HL_3) and (HH_1, HH_2, HH_3) represent the vertical, the horizontal, and the diagonal sub-bands, respectively. LL_3 indicates the approximation sub-band (approximate image), which contains identical visual data to the source image.

3.1 Fusion using blocks in the DCT domain

In any image, regions of interest (focused) are rich in information, so that will provide further clarity. Generally, variance is mostly adopted as a prevalent choice for characterizing contrast in images (Abdipour *et al*.,2016). Likewise, to verify the focused regions, we might utilize the variance as a criterion for assessing activity levels (Haghighat *et al*., 2011).

Firstly, the approximation sub-bands of the input images (LL_3^{CT}, LL_3^{MRI}) are decomposed into 8×8 nonoverlapping blocks. Then we calculate the two-dimensional DCT coefficients for each individual block. Based onEquation 8, it is very simple to measure the variance in identical blocks.

$$\sigma^2 = \frac{1}{N^2} \sum_{i=0}^{N-1} \sum_{j=0}^{N-1} [b^2(i,j) - \mu^2] \quad (7)$$

$$\sigma^2 = \sum_{k=0}^{N-1} \sum_{l=0}^{N-1} \frac{F^2(k,l)}{N^2} - \hat{F}^2(0,0) \quad (8)$$

As a result, the variance value of an $N \times N$ block can be calculated as the sum of squared normalized AC coefficients in the DCT domain.

The blocks that have the highest variance value are then chosen as the appropriate blocks in the combined approximation sub-band (LL_3^F). The goal of consistency verification (CV) (Manjunath *et al*., 1995) with 3×3 neighborhood window, for the combined approximation sub-band is that if the majority of the surrounding blocks are selected from an MRI image and the center block is selected from a CT image, the center block is switched by the same block from the MRI image, and vice versa.

3.2 Fusion using pixel significance in the ILWT domain

In the majority of image fusion techniques employing weight averaging as a fusion rule (Shah *et al*., 2011; Shah *et al*., 2013; Kumar, 2013), all pixels of the input images will participate in calculating weights, it has negative consequences for the final image quality. Avoiding this issue, we change the approximate sub-bands of the CT and MRI images using their fused. After that, we compute the optimal weighted average.

As a result of the down-sampling operation inherent in the DWT multiresolution decompositions, each coefficient located in the third level of the hierarchy exhibits a heightened degree of correlation with local neighborhoods, encompassing 2×2 windows of coefficients in the second level and 4×4 windows of coefficients in the first level. Also, every coefficient located in the second level exhibits a heightened degree of correlation with local neighborhoods, encompassing 2×2 windows of coefficients in the first level. On the third level, weights can be computed by taking the mean energy of 3×3 neighborhood windows.

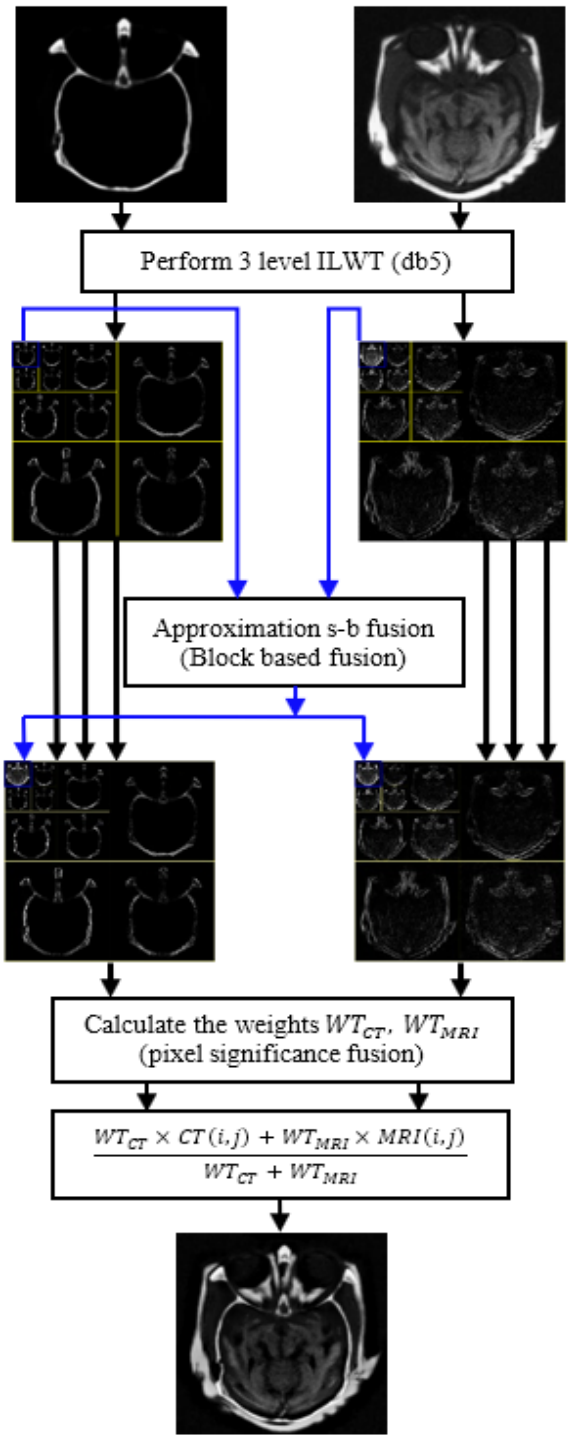

Figure 2 - The general framework of the proposed fusion method.

For simplification, we will denote the detail sub-bands as SB_L, where SB means the detail sub-bands (HL, LH, HH) and L reflects the decomposition level. The weighting coefficient associated with any detail sub-band coefficient, denoted as (WT_{SB_L}) can be meticulously computed via the following expression:

$$WT_{SB3}(i,j) = |SB_3(i,j)| + \sum_{k=0}^{1}\sum_{l=0}^{1}|SB_2(2i-k, 2j-l)| + \sum_{m=0}^{3}\sum_{n=0}^{3}|SB_1(4i-m, 4j-n)| \quad (9)$$

$$WT_{SB2}(i,j) = |SB_2(i,j)| + \sum_{k=0}^{1}\sum_{l=0}^{1}|SB_1(2i-k, 2j-l)| \quad (10)$$

$$WT_{SB1}(i,j) = \frac{1}{3^2} \times \sum_{m=-1}^{1} \sum_{n=-1}^{1} [SB_1(i-m, j-n)]^2 \quad (11)$$

Now, every coefficient in the approximation sub-band (LL_3) is correlated with the comparable coefficients in the detail sub-bands (HL_3, LH_3, HH_3). The weight factor is given below:

$$WT_{LL3}(i,j) = WT_{HL3}(i,j) + WT_{LH3}(i,j) + WT_{HH3}(i,j) \quad (12)$$

These weighting coefficients are systematically computed across all sub-bands for both CT and MRI images. Denoting the weights of the respective pixels in $CT(i,j)$ and $MRI(i,j)$ as WT_{CT} and WT_{MRI} are the weights of the corresponding pixels The fused coefficient $f(i,j)$ can be meticulously derived as the optimal weighted mean of the weight pairs (WT_{CT}, WT_{MRI}) ,as elucidated by Equation 13:

$$f(i,j) = \frac{WT_{CT} \times CT(i,j) + WT_{MRI} \times MRI(i,j)}{WT_{CT} + WT_{MRI}} \quad (13)$$

Finally, the resulting image may be generated by applying the backward ILWT to the fused (combined) coefficients $f(i,j)$.

4. Experimental results and analysis

In this part, considerable experiments are implemented in order to evaluate the performance of our approach. We use a medical image dataset that is available on the website http://www.med.harvard.edu. Our suggested medical image fusion technique is compared with other methods, like the DWT described in (Manjunath *et al*., 1995), SIDWT cited in (Rockinger, 1997), PCA approach in (Kwarteng *et al*., 1989), Laplacian pyramids technique presented in (Burt *et al*., 1983), DCT+Ac_Max (Phamila *et al*.,2014) and DWT+Pca_av (Vijayarajan *et al*.,2015). We consider the Standard deviation (STD), entropy (He), average gradient (AG) and spectral frequency (SF) as objective fusion metrics. Also, the edge-based similarity metric $(Q^{\frac{AB}{F}})$ and the total loss of information $(L^{\frac{AB}{F}})$ are objective fusion metrics.

4.1 Qualitative analysis

In this part, we empirically demonstrate the superior perceptual visual quality and diagnostic efficacy inherent in the resulting fused medical images generated by our innovative method in contrast to the previously mentioned techniques.

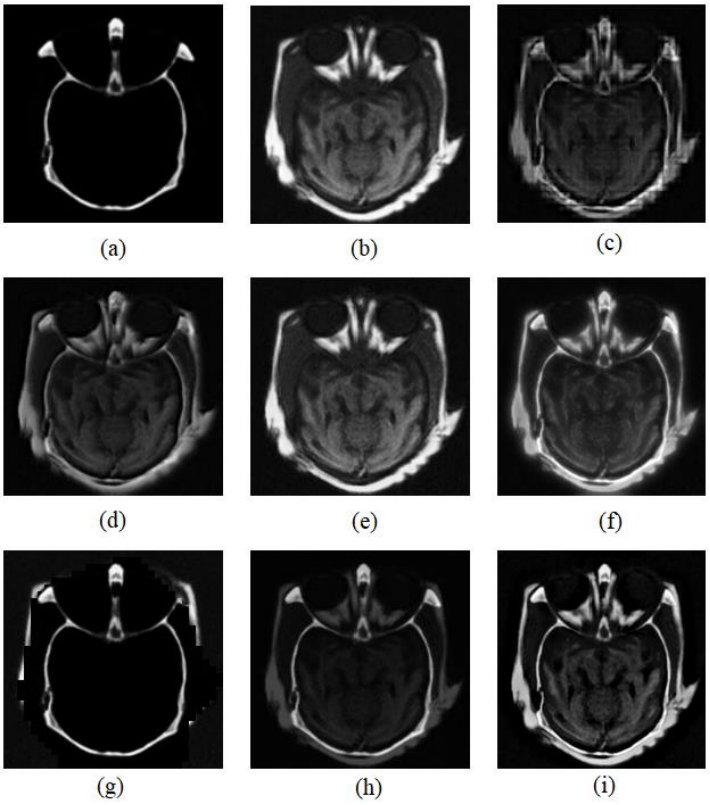

Figure 3 - Visual quality of the fused images of: (a) CT (b) MRI (c) DWT (d) SIDWT (e) PCA (f) LAP (g) DCT_Acmax (h) DWT_Pca (i) Proposed.

As shown in Figure 3, a and b represent brain images taken through CT and MRI modalities, respectively. CT is highly effective for imaging and characterizing hard tissues and dense structures like bones. While MRI is able to describe the brain, it excels at delivering exceptional contrast between various soft tissues within the brain. This capability extends to the discernment of fine structural intricacies within these soft tissues. Nevertheless, for better treatment and diagnosis of an illness, it is imperative to combine all pertinent information from both images into a unified representation through the fusion procedure. Fig.3c represents the fused image of the DWT method. Fused images of SIDWT, PCA, LAP, DCT_Acmax and DWT_Pca methods are displayed in Figure 3 d-h, respectively. The fused image resulting from the application of the introduced method is shown in Figure 3i.

Form these outcomes; it is clearly evident that the visual quality of the resulting image of the DWT suffers from some distortion due to the Gibbs phenomenon (see Figure 3c). Also, the resulting image of the DCT_Acmax method suffers from blocking artefacts because images in the DCT domain are divided into blocks (see Figure 3g). SIDWT, LAP and DWT_Pca methods introduce some reduction in contrast (especially in soft tissue) into the fused image. Whereas the PCA method cannot carry out the fusion process. Quite the contrary, the proposed method gives fused results by making full use of the two input images and can also clearly express the soft tissue and bone information simultaneously. The resulting image shows superior visual quality compared to the results achieved by other methods.

4.2 Quantitative analysis

The quantitative evaluation of our introduced approach in comparison with some fusion approaches (cited above) is performed through the utilization of a suite of fusion quality metrics such as STD, AG, He, SF, $Q^{\frac{AB}{F}}$ and $L^{\frac{AB}{F}}$.

The contrast level inherent in an image is measured by the STD metric. The AG metric serves as an evaluative parameter for assessing the sharpness, clarity, and acuity characteristics of an image. The He measure serves as a quantitative metric, showing the extent to which data from the two source images has been transferred and incorporated into the amalgamated image. The SF metric functions as an assessment tool for measuring the overall activity level within the resulting fused image. It is used to evaluate and quantify the variations in pixel intensities across different spatial frequencies within an image. It helps in understanding the image's patterns, texture, and overall structure. $Q^{\frac{AB}{F}}$ and $L^{\frac{AB}{F}}$ metrics provide quantitative insights into the edge information dynamics during image fusion. The $Q^{\frac{AB}{F}}$ quantifies the amount of edge information effectively transferred from the source images to the fused image, while the $L^{\frac{AB}{F}}$ measures the extent of edge information loss in the fusion process. To achieve superior performance, any method should exhibit high values for most metrics, with the notable exception of the $L^{\frac{AB}{F}}$ metric.

In Table I, a comprehensive performance evaluation of various image fusion methods is presented, including the introduced approach designed for CT and MRI medical images. This assessment includes a thorough examination and analysis of their respective capabilities and results. It has been noted that the DWT_Pca method exhibits the most minimal values for SD, AG and $Q^{\frac{AB}{F}}$ metrics, and a higher value for $L^{\frac{AB}{F}}$ metrics. The DCT_Acmax method has the lowest He value. The SF metric value is low for the SIDWT method. In most metrics, our proposed method has maximum performance; this observation indicates that the fused image possesses a heightened level of contrast, is clearer, is sharper and has with more visual information. Furthermore, it is noteworthy that the proposed algorithm excels at preserving information from the source images.

Table 1 – Quantitative evaluation of the fused images.

	Measures					
Methods	**SD**	**AG**	**He**	**SF**	$Q^{AB/F}$	$L^{AB/F}$
DWT	38.02	7.906	6.169	14.74	0.638	0.346
SIDWT	35.33	6.174	6.070	11.46	0.561	0.434
PCA	54.24	7.647	6.549	13.75	0.634	0.365
LAP	51.22	7.539	6.546	14.08	0.768	0.227
DCT_Acmax	39.92	5.789	3.660	**17.98**	0.549	0.442
DWT_Pca	31.92	4.870	5.340	11.60	0.524	0.475
Proposed	**57.63**	**10.02**	**6.770**	17.02	**0.777**	**0.206**

5. Conclusion

A novel image fusion method is proposed, designed to combine the multifaceted datasets derived from computed tomography (CT) and magnetic resonance imaging (MRI) modalities, culminating in the creation of a singular composite image containing all significant visual information to provide doctors and radiologists with heightened diagnostic significance and informational content. This method hinges on leveraging the variance within the DCT domain as a discerning metric for contrast assessment. Furthermore, it exploits pixel significance within the ILWT domain as an additional crucial determinant in the fusion process.

This approach exhibits exceptional simplicity and efficiency, rendering it exceptionally well-suited for real-time applications demanding rapid processing and responsiveness because of the integer-to-integer implementation of LWT. Comprehensive experiments have been meticulously executed to empirically establish the superior efficacy of the introduced approach in comparison with several extant image fusion techniques. This assessment encompasses both qualitative and quantitative evaluations, thereby affirming the method's heightened performance and capabilities.

Our approach is exceptionally well-suited for the integration and enhancement of both CT and MRI medical imagery, affirming its aptitude for applications in this domain.

References

Abdipour, M., & Nooshyar, M. (2016). Multi-focus image fusion using sharpness criteria for visual sensor networks in wavelet domain. *Computers & Electrical Engineering, 51*, 74-88. https://doi.org/10.1016/j.compeleceng.2016.03.011.

Alseelawi, N., Hazim, H. T., & Salim ALRikabi, H. T. (2022). A Novel Method of Multimodal Medical Image Fusion Based on Hybrid Approach of NSCT and DTCWT. *International Journal of Online & Biomedical Engineering, 18(3)*. https://doi.org/10.1007/s12652-020-02293-4.

Azam, M. A., Khan, K. B., Salahuddin, S., Rehman, E., Khan, S. A., Khan, M. A., ... & Gandomi, A. H. (2022). A review on multimodal medical image fusion: Compendious analysis of medical modalities, multimodal databases, fusion techniques and quality metrics. *Computers in biology and medicine, 144*, 105253. https://doi.org/10.1016/j.compbiomed.2022.105253.

Bhalla, K., Koundal, D., Sharma, B., Hu, Y. C., & Zaguia, A. (2022). A fuzzy convolutional neural network for enhancing multi-focus image fusion. *Journal of Visual Communication and Image Representation, 84*, 103485. https://doi.org/10.1016/j.jvcir.2022.103485.

Burt, P. J., & Adelson, E. H. (1987). The Laplacian pyramid as a compact image code. *In Readings in computer vision* (pp. 671-679). Morgan Kaufmann. https://doi.org/10.1016/B978-0-08-051581-6.50065-9.

Calderbank, A. R., Daubechies, I., Sweldens, W., & Yeo, B. L. (1998). Wavelet transforms that map integers to integers. *Applied and computational harmonic analysis, 5(3)*, 332-369. https://doi.org/10.1006/acha.1997.0238.

Choi, M. (2006). A new intensity-hue-saturation fusion approach to image fusion with a tradeoff parameter. *IEEE Transactions on Geoscience and Remote sensing, 44(6)*, 1672-1682. https://doi.org/10.1109/TGRS.2006.869923.

Diwakar, M., Singh, P., & Shankar, A. (2021). Multi-modal medical image fusion framework using co-occurrence filter and local extrema in NSST domain. *Biomedical Signal Processing and Control, 68*, 102788. https://doi.org/10.1016/j.bspc.2021.102788.

Ganasala, P., & Prasad, A. D. (2020). Medical image fusion based on laws of texture energy measures in stationary wavelet transform domain. *International Journal of Imaging Systems and Technology, 30(3)*, 544-557. https://doi.org/10.1002/ima.22393.

Gharbia, R., El Baz, A. H., Hassanien, A. E., & Tolba, M. F. (2014). Remote sensing image fusion approach based on Brovey and wavelets transforms. *In Proceedings of the Fifth International Conference on Innovations in Bio-Inspired Computing and Applications IBICA 2014* (pp. 311-321). Springer International Publishing. https://doi.org/10.1007/978-3-319-08156-4_31.

Haghighat, M. B. A., Aghagolzadeh, A., & Seyedarabi, H. (2011). Multi-focus image fusion for visual sensor networks in DCT domain. *Computers & Electrical Engineering, 37(5)*, 789-797. https://doi.org/10.1016/j.compeleceng.2011.04.016.

Hou, R., Zhou, D., Nie, R., Liu, D., & Ruan, X. (2019). Brain CT and MRI medical image fusion using convolutional neural networks and a dual-channel spiking cortical model. *Medical & biological engineering & computing, 57*, 887-900. https://doi.org/10.1007/s11517-018-1935-8.

Shreyamsha Kumar, B. K. (2013). Multifocus and multispectral image fusion based on pixel significance using discrete cosine harmonic wavelet transform. *Signal, Image and Video Processing, 7*, 1125-1143. https://doi.org/10.1007/s11760-012-0361-x.

Kwarteng, P., & Chavez, A. (1989). Extracting spectral contrast in Landsat Thematic Mapper image data using selective principal component analysis. *Photogramm. Eng. Remote Sens, 55(1)*, 339-348.

Latreche, B., Saadi, S., Kious, M., & Benziane, A. (2019). A novel hybrid image fusion method based on integer lifting wavelet and discrete cosine transformer for visual sensor networks. *Multimedia Tools and Applications, 78*, 10865-10887. https://doi.org/10.1007/s11042-018-6676-z.

Li, H., Manjunath, B. S., & Mitra, S. K. (1995). Multisensor image fusion using the wavelet transform. *Graphical models and image processing, 57(3)*, 235-245. https://doi.org/10.1006/gmip.1995.1022.

Li, S., Kang, X., Fang, L., Hu, J., & Yin, H. (2017). Pixel-level image fusion: A survey of the state of the art. *information Fusion, 33*, 100-112. https://doi.org/10.1016/j.inffus.2016.05.004.

Li, X., & Zhao, J. (2021). A novel multi-modal medical image fusion algorithm. *Journal of Ambient Intelligence and Humanized Computing, 12*, 1995-2002. https://doi.org/10.3991/ijoe.v18i03.28011.

Liu, Y., Wang, L., Cheng, J., Li, C., & Chen, X. (2020). Multi-focus image fusion: A survey of the state of the art. *Information Fusion, 64*, 71-91. https://doi.org/10.1016/j.inffus.2020.06.013.

Metwalli, M. R., Nasr, A. H., Allah, O. S. F., & El-Rabaie, S. (2009, December). Image fusion based on principal component analysis and high-pass filter. *In 2009 International Conference on Computer Engineering & Systems* (pp. 63-70). IEEE. https://doi.org/10.1109/ICCES.2009.5383308.

Na, Y., Zhao, L., Yang, Y., & Ren, M. (2018). Guided filter-based images fusion algorithm for CT and MRI medical images. *IET Image Processing, 12(1)*, 138-148. https://doi.org/10.3991/ijoe.v18i03.28011.

Phamila, Y. A. V., & Amutha, R. (2014). Discrete Cosine Transform based fusion of multi-focus images for visual sensor networks. *Signal Processing, 95*, 161-170. https://doi.org/10.1016/j.sigpro.2013.09.001.

Rockinger, O. (1997, October). Image sequence fusion using a shift-invariant wavelet transform. *In Proceedings of international conference on image processing* (Vol. 3, pp. 288-291). IEEE. https://doi.org/10.1109/ICIP.1997.632093.

Sahu, A., Bhateja, V., & Krishn, A. (2014, November). Medical image fusion with Laplacian pyramids. *In 2014 International conference on medical imaging, m-health and emerging communication systems (MedCom)* (pp. 448-453). IEEE. https://doi.org/10.1109/MedCom.2014.7006050.

Shah, P., Merchant, S. N., & Desai, U. B. (2013). Multifocus and multispectral image fusion based on pixel significance using multiresolution decomposition. *Signal, Image and Video Processing, 7*, 95-109. https://doi.org/10.1007/s11760-012-0361-x.

Shah, P., Srikanth, T. V., Merchant, S. N., & Desai, U. B. (2011, June). A novel multifocus image fusion scheme based on pixel significance using wavelet transform. *In 2011 IEEE 10th IVMSP Workshop: Perception and Visual Signal Analysis* (pp. 54-59). IEEE. https://doi.org/10.1109/IVMSPW.2011.5970354.

Singh, R., & Khare, A. (2014). Fusion of multimodal medical images using Daubechies complex wavelet transform–A multiresolution approach. *Information fusion, 19*, 49-60. https://doi.org/10.1016/j.inffus.2012.09.005.

Singh, S., Anand, R. S., & Gupta, D. (2018). CT and MR image information fusion scheme using a cascaded framework in ripplet and NSST domain. *IET Image Processing, 12(5)*, 696-707. https://doi.org/10.1049/iet-ipr.2017.0214.

Starmans, M., van der Voort, S. R., Phil, T., Timbergen, M. J., Vos, M., Padmos, G. A., ... & Klein, S. (2021). Reproducible radiomics through automated machine learning validated on twelve clinical applications. *arXiv preprint arXiv:2108*.08618. https://doi.org/10.1007/s10278-022-00590-2.

Sweldens, W. (1998). The lifting scheme: A construction of second generation wavelets. *SIAM journal on mathematical analysis, 29(2)*, 511-546. https://doi.org/10.1137/S0036141095289051.

Ursuleanu, T. F., Luca, A. R., Gheorghe, L., Grigorovici, R., Iancu, S., Hlusneac, M., ... &

Grigorovici, A. (2021). The use of artificial intelligence on segmental volumes, constructed from MRI and CT images, in the diagnosis and staging of cervical cancers and thyroid cancers: a study protocol for a randomized controlled trial. *Journal of Biomedical Science and Engineering*, *14(6)*, 300-304. https://doi.org/10.4236/jbise.2021.146025.

Vijayarajan, R., & Muttan, S. (2015). Discrete wavelet transform based principal component averaging fusion for medical images. *AEU-International Journal of Electronics and Communications*, *69(6)*, 896-902. https://doi.org/10.1016/j.aeue.2015.02.007.

Wan, Z., Dong, Y., Yu, Z., Lv, H., & Lv, Z. (2021). Semi-supervised support vector machine for digital twins based brain image fusion. *Frontiers in Neuroscience*, *15*, 705323. https://doi.org/10.3389/fnins.2021.705323.